Published in final edited form as:

*Clin Cancer Res*. 2019 January 01; 25(1): 277–289. doi:10.1158/1078-0432.CCR-18-1544.

# Combined blockade of activating *ERBB2* mutations and ER results in synthetic lethality of ER+/HER2 mutant breast cancer

**Sarah Croessmann**[1], **Luigi Formisano**[1], **Lisa N. Kinch**[2], **Paula I. Gonzalez-Ericsson**[3], **Dhivya R. Sudhan**[1], **Rebecca J. Nagy**[4], **Aju Mathew**[5], **Eric H. Bernicker**[6], **Massimo Cristofanilli**[7], **Jie He**[8], **Richard E. Cutler Jr**[9], **Alshad S. Lalani**[10], **Vincent A. Miller**[11], **Richard B. Lanman**[4], **Nick V. Grishin**[2,10], and **Carlos L. Arteaga**[1,3,11]

[1]Department of Medicine Vanderbilt-Ingram Cancer Center, Vanderbilt University Medical Center, Nashville, TN;

[2]Howard Hughes Medical Institute, UT Southwestern Medical Center, Dallas, TX;

[3]Department of Breast Cancer Program, Vanderbilt-Ingram Cancer Center, Vanderbilt University Medical Center, Nashville, TN;

[4]Guardant Health, Inc., Redwood, CA;

[5]University of Kentucky Markey Cancer Center, Lexington, KY;

[6]Houston Methodist Cancer Center, Houston, TX;

[7]Lurie Comprehensive Cancer Center, Chicago, IL;

[8]Foundation Medicine, Inc., Cambridge, MA;

[9]Puma Biotechnology, Inc., Los Angeles, CA;

[10]Departments of Biophysics and Biochemistry, UT Southwestern Medical Center, Dallas, TX

[11]Department of Cancer Biology, Vanderbilt-Ingram Cancer Center, Vanderbilt University Medical Center, Nashville, TN;

## Abstract

**Purpose:** We examined the role of *ERBB2* activating mutations in endocrine therapy resistance in estrogen receptor positive (ER+) breast cancer.

**Design:** *ERBB2* mutation frequency was determined from large genomic databases. Isogenic knock-in *ERBB2* mutations in ER+ MCF7 cells and xenografts were used to investigate estrogen-independent growth. Structural analysis was used to determine the molecular interaction of $HER^{L755S}$ with HER3. Small molecules and siRNAs were used to inhibit PI3Kα, TORC1 and HER3.

*Corresponding Author: Carlos L. Arteaga, MD, UTSW Simmons Comprehensive Cancer Center, 5323 Harry Hines Blvd., Dallas, TX 75390-8590, carlos.arteaga@utsouthwestern.edu, Tel. 214-648-1677, Fax 214-648-7084.

**Disclosure of potential conflicts of interest:** R.C. and A.L. are employees of Puma Inc. R.N. and R.L. are employees of Guardant Health. J.H. and V.M. are employees of Foundation Medicine.

**Results:** Genomic data revealed a higher rate of *ERBB2* mutations in metastatic vs. primary ER+ tumors. MCF7 cells with isogenically incorporated *ERBB2* kinase domain mutations exhibited resistance to estrogen deprivation and to fulvestrant both *in vitro* and *in vivo*, despite maintaining inhibition of ERα transcriptional activity. Addition of the irreversible HER2 tyrosine kinase inhibitor neratinib restored sensitivity to fulvestrant. HER2-mutant MCF7 cells expressed higher levels of p-HER3, p-AKT and p-S6 than cells with wild type HER2. Structural analysis of the HER2$^{L755S}$ variant implicated a more flexible active state, potentially allowing for enhanced dimerization with HER3. Treatment with a PI3Kα inhibitor, a TORC1 inhibitor or HER3 siRNA, but not a MEK inhibitor, restored sensitivity to fulvestrant and to estrogen deprivation. Inhibition of mutant HER2 or TORC1, when combined with fulvestrant, equipotently inhibited growth of MCF7/*ERBB2*$^{V777L}$ xenografts, suggesting a role for TORC1 in antiestrogen resistance induced by *ERBB2* mutations.

**Conclusions:** *ERBB2* mutations hyperactivate the HER3/PI3K/AKT/mTOR axis, leading to antiestrogen resistance in ER+ breast cancer. Dual blockade of the HER2 and ER pathways is required for the treatment of ER+/HER2 mutant breast cancers.

**Translational Significance—***ERBB2* activating mutations occur with increased frequency in ER+ breast cancers after progression on antiestrogen therapy. Inhibition of mutant HER2 function with neratinib restores the efficacy of antiestrogen therapy. Thus, we propose dual blockade of the HER2 and ER pathways is required for the treatment of ER+/HER2 mutant breast cancers.

## Introduction

Estrogen-receptor positive (ER+) breast cancer is the most common breast cancer subtype, representing about 80% of all patients. Endocrine therapies, such as selective ER modulators (SERMs; i.e., tamoxifen), selective ER down-regulators (SERDs; i.e., fulvestrant), and estrogen suppression with aromatase inhibitors (AIs), are standard of care treatment for patients with advanced ER+ breast cancer. Many large randomized clinical trials have proven the effectiveness of these therapies in preventing metastatic recurrence (1,2). However, about 20% of patients diagnosed with operable ER+ tumors will recur during or after adjuvant endocrine therapy. Despite the overall efficacy of these therapies, mortality from antiestrogen-resistant ER+ tumors still accounts for the majority of breast cancer deaths each year. Up to now, the only mechanisms of antiestrogen resistance that are supported in the clinic are HER2 amplification (3,4), mutations in the ligand-binding domain (LBD) of *ESR1* (5,6), and dysregulation of the CDK4/6 pathway (7).

Human epidermal growth factor receptor 2 (*ERBB2*/HER2) is frequently altered via gene amplification in breast cancer. Some ER+ breast cancers may gain HER2 amplification and/or overexpression as a result of treatment pressures and/or tumor evolution (4). This may allow amplified HER2 signaling to drive tumor progression, thus reducing the dependence of a tumor on ER while also inducing resistance to antiestrogen therapy (3,8,9). The ERBB family of transmembrane receptor tyrosine kinases (RTKs) consists of EGFR (ERBB1), HER2 (ERBB2), HER3 (ERBB3), and HER4 (ERBB4). Binding of ERBB ligands to the extracellular domain of EGFR, HER3, and HER4 induces the formation of kinase active hetero-oligomers (10). HER2 does not bind ERBB ligands directly, but it is in a conformation that resembles a ligand-activated state and favors dimerization (11,12).

Activation of HER2 induces transphosphorylation of the ERBB dimer partner and stimulates several intracellular pathways such as RAS/RAF/MEK/ERK, PI3K/AKT/TOR, Src kinases, and STAT transcription factors [reviewed in (13)]. Activation of these pathways allows for extensive crosstalk with ER transcriptional activity, potentially leading to endocrine resistance.

*ERBB2* missense mutations have been found in approximately 2–4% of breast cancers (14,15), occurring with higher frequency in metastatic tumors (cBioPortal). Activating *ERBB2* mutations occur most commonly in the kinase and extracellular domains in the absence of HER2 amplification (14–18). Among all *ERBB2* missense mutations in breast cancer, approximately 70% occur in ER+ breast cancers and close to 80% of these occur in the kinase domain (cBioPortal). Herein, we report that *ERBB2* missense mutations occur at a significantly higher frequency in metastatic disease, thus suggesting these variants are acquired as a mechanism of resistance to endocrine therapy. Our studies also demonstrate that *ERBB2* mutations hyperactivate HER3 and the phosphoinositide 3-kinase PI3K/AKT/mTOR signaling pathway. In turn, this results in estrogen-independent growth and resistance to endocrine therapy. Based on these data, we posit that dual targeting of activating *ERBB2* mutations or their downstream effectors, HER3/PI3K, and the ER pathway is necessary for optimal growth inhibition of ER+/HER2 mutant breast cancers.

## Materials and Methods

### Cell lines.

The ER+ breast cancer cell line MCF-7 (ATCC® HTB-22™) was previously isogenically modified using AAV-mediated gene targeting to include three *ERBB2* missense mutations (G309A, L755S, V777L) and maintained as previously described (18). Cell lines were not carried past 20 passages.

### Determination of ER status and *ERBB2* mutations.

ER status of *ERBB2* mutants was determined using databases from cBioPortal (cohorts include TCGA, METABRIC, GENIE, MBC Project, France 2016) and databases from Foundation Medicine. The frequency of *ERBB2* mutations in primary and metastatic tumors was determined using cBioPortal (cohorts listed above, tissue-based) and databases from Guardant Health (plasma-based). Several selected patients from the Guardant Health database were analyzed for allelic frequency as a function of treatment course.

### Cell growth assay.

Clonogenic growth assays to determine resistance to estrogen deprivation or to fulvestrant were performed in 10 cm dishes. Drug sensitivity assays were carried out in 12-well dishes at a seeding density of 2,000 cells/well. Plates were stained using crystal violet. Cell growth was quantified using both a LI-COR Odyssey Infrared plate reader of stained monolayers and cell numbers measured with a Coulter Counter. For experiments with siRNAs, cells were reverse-transfected with HER3 siRNAs or scrambled control (Cell Signaling) according to the Lipofectamine RNAiMAX protocol (Invitrogen). The next day 2,000 cells/well were reseeded in full medium ± 1 μM fulvestrant or estrogen-free medium ± 1 nM

estradiol. Cells were counted on days 0, 3, and 6 after plating. For assessment of HER3 levels, cells were harvested 3 days post transfection and cell lysates were subjected to immunoblot analysis.

### Combinatorial Drug Screen.

Cells were seeded at a density of 3000 cells/well into 96-well plates in triplicate and treated with a dose range (0, 31.25 nM, 62.5 nM, 125 nM, 250 nM, 500 nM, and 1000 nM) of fulvestrant and neratinib each. Media was replenished every other day. At the end of 5 days, cells were fixed and stained with crystal violet. Stained monolayers were lysed in 1% SDS and read at an absorbance of 560 nm using a GloMax Plate reader. Combination Index values were calculated for the dose combination 1 μM fulvestrant and 250 nM neratinib using the computer program CompuSyn. Values less than 1 indicate a synergistic interaction.

### Acinar morphogenesis assay.

Three-dimensional (3D) morphogenesis assays were carried out as previously described (18). Briefly, cells were seeded in growth factor-reduced Matrigel (BD Biosciences) in the absence of estradiol in 8-well chamber slides at a density of $2.5 \times 10^4$ cells/mL. Chambers were supplemented with 1 nM estradiol, 1 μM fulvestrant, and/or 200 nM neratinib. Chambers were imaged with an Olympus DP20 microscope on day 14.

### Immunoblot analysis.

Cells were washed with PBS and lysed on ice in NP-40 lysis buffer plus protease and phosphatase inhibitors. Protein concentration in cell lysates was measured using BCA protein assay reagent (Pierce). Lysates were subjected to SDS-PAGE followed by transfer to nitrocellulose membranes (Invitrogen) as previously described (19). Primary antibodies included: p-HER2 Y1248 (Millipore 06–229), HER2 (CS2242), p-HER3 Y1197 (CS4561), HER3 (CS12708), PathScan Multiplex Western Cocktail I (for p-AKT S473, p-p90RSK, p-ERK, and p-S6), p-S6K (CS9205), AKT (CS9272), ERK (CS9102), S6K (CS9202), p90RSK (CS9333), S6 (CS2217), p-ERα S167 (SC-101676), ERα (SC-73479), GAPDH (CSXP5174). Immunoreactive bands were detected by enhanced chemiluminescence following incubation with horseradish peroxidase-conjugated secondary antibodies. The Invitrogen NuPage system was used. Nitrocellulose membranes were cut horizontally to probe with multiple antibodies.

### Transcriptional reporter assays.

Cells were plated in 96-well plates at a density of 4,000 cells/well in IMEM media with 10% charcoal-stripped serum; 24 h later, cells were transfected with pERE (Estrogen Responsive Elements)-luciferase and pCMV-Renilla plasmids. 24 h post-transfection, cells were treated with vehicle (control), 1 nM estradiol, 1 μM fulvestrant, and/or 200 nM neratinib. Luciferase activity was measured 24 to 48 h later using the Dual Luciferase Kit (Promega) according to the manufacturer's instructions utilizing the Promega GloMax plate reader.

### Gene expression analyses.

Gene expression analysis was performed as previously described (20). Briefly, cells were plated in estrogen-free media in triplicate. Cells were harvested and RNA was purified using the RNeasy Kit (Qiagen). cDNA was generated using High-Capacity cDNA Reverse Transcription Kits (Applied Biosystems) and analyzed using the Estrogen Receptor PCR Array (Qiagen, PAHS-005Z).

### Xenograft studies.

Mouse experiments were approved by the Vanderbilt Institutional Animal Care and Use Committee. Female ovariectomized athymic mice were implanted with a 14-day release 17β-estradiol (E2) pellet (0.17 mg). 24 h later, $5 \times 10^6$ MCF-7 cells harboring a *ERBB2* L755S or V777L mutation, as indicated, suspended in PBS and Matrigel (BD Biosciences) at a 1:1 ratio were injected subcutaneously (s.c.) into the dorsum of each mouse. Approximately 4 weeks later, mice bearing tumors of ≥150 $mm^3$ were randomized to treatment with vehicle (control), neratinib (40 mg/kg/day via orogastric gavage – o.g.), fulvestrant (5 mg/wk, s.c.), everolimus (5 mg/kg/day, o.g.), and/or alpelisib (30 mg/kg/day, o.g.), as indicated. Tumor volume in $mm^3$ was measured 2 times a week by using the formula: volume = $width^2$ x length/2. Portions of tumors were snap frozen or fixed in 10% neutral-buffered formalin and embedded in paraffin for subsequent analyses. Five-micron paraffinized sections were used for IHC using a phospho-S6 antibody (Cell Signaling 2211). Sections were scored by an expert pathologist (PLG-E) blinded to treatment arm. Fulvestrant was kindly provided by AstraZeneca Pharmaceuticals.

### Immunoprecipitation.

Cell lysates were harvested using ice cold lysis buffer [1% NP-40, 20 mM Tris pH 7.4, 10% Glycerol, 150 mM NaCL, 1 mM EDTA, 1 mM EGTA, 5 mM sodium pyrophosphate, 50 mM NaF, 10 mM β-glycerophosphate, protease and phosphatase inhibitor cocktails (Sigma-Aldrich)] and rotated at 4°C for 1 h. Lysates were then clarified by spinning at 10,000 xg at 4°C for 15 min. Protein concentrations were measured using BCA standard curves (Pierce). Lysates were pre-cleared with 50 μL of Protein G agarose beads (Life technologies 10003D) at 4°C for 1 h. Immunoprecipitation was carried out using the Invitrogen Immunoprecipitation Kit (10004D) as directed. Lysates were next subjected to SDS-PAGE and immunoblot analysis. Immunoblots were quantified using ImageJ software.

### Structural Analysis.

Known EGFR-like structures were identified using either HHPRED search of the PDB with the HER2 kinase domain query sequence (SwissProt sequence P04626.1, residue range 685–1255) or BLAST sequence search (21) of all protein kinase-like domain sequences defined in ECOD (Evolutionary Classification Of structure Domains) (22). Kinase structure domains outlined in ECOD were defined manually as active or inactive based on the position of the regulatory C helix and the proximity of the K753/E770 sidechains (numbered according to HER2), whose ion pair interaction are a hallmark of protein kinase activation. Manually defined active and inactive conformations were double checked using Dali superpositions. The flexibility of residue positions corresponding to HER2 L755 were assessed using the

structure B-factor of the Cα atom for all identified EGFR-like kinase structures containing coordinates for that residue. B-factors were normalized by the Z-score of the PBD, where the mean and standard deviation are calculated from all Cα atoms in the same chain. Accessible surface (Gerstein) of wild type (WT) EGFR (pdb 4riw, chain B) and mutant (pdb 4riw, chain B, L723 replaced with Ser) structures were calculated with default parameters (23). Changes in calculated surface exposure between WT and mutant were compared for all residues, with those surrounding the mutation becoming increasingly exposed. The stability scores resulting from mutating L755S in the background of WT EGFR and HER2 crystal structures, as well as HER2 structure models based on EGFR templates, were assessed with the Site Directed Mutator (SDM) server (24), which calculates a potential energy function based on the environment-specific amino acid substitution frequencies within homologous protein families.

### Statistical analysis.

All experiments were performed using three technical replicates and at least two independent times. P values were calculated using GraphPad Prism (version 6.0) by ANOVA followed by Tukey multiple comparisons test.

## Results

### *ERBB2* mutations commonly occur in ER+ breast cancer after progression on endocrine therapy.

Interrogation of cBioPortal and Foundation Medicine databases found that approximately 70% of *ERBB2* mutations are detectable in ER+/HER2 non-amplified breast cancers, with the majority of them occurring in the kinase domain (Supp. Table S1). Further interrogation of several genomic databases available through the cBioPortal interface (TCGA, METABRIC, GENIE, MBC Project, France 2016), as well as cancer patients' plasma specimens in the Guardant Health database, showed a significantly higher occurrence of *ERBB2* mutations in patients with metastatic disease vs. primary tumors (Figure 1A). Within the GENIE database, the percentage of *ERBB2* mutations in metastatic biopsies (4.3%) almost doubled that in primary cancers (2.5%), altogether suggesting they are an acquired mechanism of antiestrogen therapy resistance. This was further supported by plasma ctDNA analysis from a small cohort of patients with ER+/HER2-negative (HER2 non-amplified) breast cancer in the Guardant Health database (Figure 1B). Comparison between pre-treatment and post-progression on endocrine therapy showed the emergence and/or an increase in the allelic frequency of activating *ERBB2* mutations. An in-depth mutational analysis of tumors from patient 1, harboring the L755S mutation, and patient 2, harboring the V777L mutation, showed the emergence of the *ERBB2* mutations as a dominant alteration in later samples (Figure 1C, D). Interrogation of online databases demonstrated that *ERBB2* mutations were mutually exclusive with *ESR1* mutations, a mechanism of escape from hormone dependence (Supp. Figure S1). This suggests that *ERBB2* mutations operate independently of the ER pathway in the development of antiestrogen resistance.

In a case study of a postmenopausal woman with advanced ER+ breast cancer who had progressed after multiple endocrine therapies and was considered resistant to antiestrogens, next gene sequencing (NGS) of DNA from a skin metastasis revealed a *ERBB2* L869R activating mutation (Figure 1E). The patient was placed on neratinib monotherapy and, after exhibiting an excellent clinical response, progressed with bone and lymph node metastases (16). Addition of the ER antagonist fulvestrant to neratinib resulted to in significant and prolonged tumor regression suggesting that ER+ breast cancers with *ERBB2* activating mutations may require this therapeutic combination.

### Activating *ERBB2* mutations generate resistance to anti-ER therapies.

To determine if *ERBB2* missense mutations are causally associated with endocrine therapy resistance we used ER+ MCF7 breast cancer cells that had been isogenically modified to contain three relatively common *ERBB2* missense mutations in the cell's genome; G309A in the extracellular domain (ECD), and L755S and V777L, both in the kinase domain (KD) (18). Isogenic cell lines were previously developed using AAV-mediated gene targeting which incorporates the desired point mutation into the host cell's genome through homologous recombination. Mutations were incorporated into a single allele and expressed under the cell's endogenous promoter. This provides a biologically relevant model that best mimics mutations in primary tumors. MCF7s require estrogen in order to propagate exponentially. $MCF7^{L755S}$ and $MCF7^{V777L}$ cells but not cells with the ECD mutation, $MCF7^{G309A}$, or cells with WT HER2 exhibited robust growth in the absence of estradiol (Figure 2A), a scenario akin to that of a post-menopausal patient treated with aromatase inhibitors. Establishment of long-term estrogen deprived (LTED) stable cell lines showed similar trends with MCF7 cells harboring both KD mutations propagating early in the absence of estradiol. Conversely, $MCF7^{WT}$ and $MCF7^{G309A}$ cells exhibited near complete growth arrest and required 20+ days before achieving confluence (Figure 2B, C).

Similarly, $MCF7^{L755S}$ and $MCF7^{V777L}$ cells were resistant to the selective estrogen receptor degrader (SERD) fulvestrant whereas $MCF7^{WT}$ and $MCF7^{G309A}$ cells were growth inhibited >90% compared to untreated controls (Figure 2D). Development of fulvestrant resistant lines exhibited trends nearly identical to the development of the LTED lines (Supp. Figure S2). Fulvestrant was still able to downregulate ER protein levels as well as inhibit ligand-independent and estradiol-induced ER reporter activity in all four cell types (Figure 2E, F), suggesting the resistance associated with the *ERBB2* KD mutations was not explained by loss of fulvestrant's action on ER.

### Dual blockade of ER and HER2 is required to inhibit growth of ER+/*HER2*-mutant breast cancer cells.

We next investigated the effect of the pan-HER irreversible tyrosine kinase inhibitor (TKI) neratinib alone or in combination with fulvestrant on cells with WT or mutant HER2. MCF7 cells with WT HER2 and with the ECD mutation showed a near complete response to fulvestrant alone, while cells harboring the two KD mutations responded only partially. Treatment with neratinib partially inhibited proliferation of all three cells harboring knock-in *ERBB2* mutations. Since low levels of WT HER2 play no oncogenic role in MCF7 cells, neratinib was inactive against $MCF7^{WT}$ cells (Figure 3A). Complete growth inhibition of the

HER2 mutant cells was only observed upon treatment with both neratinib and fulvestrant, further suggesting that in ER+ tumors harboring activating *ERBB2* mutations, both ER and HER2 signaling drive cell viability. To determine if neratinib and fulvestrant were synergistic, a dose range (0, 31.25 nM, 62.5 nM, 125 nM, 250 nM, 500 nM, and 1000 nM) of each drug alone and in combination was analyzed to calculate the combination index. For the combination of 250 nM of neratinib and 1 μM of fulvestrant, $MCF7^{V777L}$ cells (Figure 3B) and $MCF7^{L755S}$ cells (Supp. Figure S3) exhibited a combination index of 0.22 and 0.49, respectively, both of which are considered synergistic. Similar results to the 2D *in vitro* assays were observed in 3D-matrigel. $MCF7^{L755S}$ and $MCF7^{V777L}$ cells formed large invasive irregular acini in the absence of estrogen, which were ablated by the addition of neratinib, consistent with a transformed phenotype driven by aberrant HER2 signaling (Figure 3C, top two rows). Picomolar concentrations of estradiol rescued $MCF7^{L755S}$ and $MCF7^{V777L}$ from the effect of the HER2 TKI; addition of fulvestrant to estradiol and neratinib restored acinar growth inhibition, further supporting dual ER and HER2 blockade are required to ablate their invasive phenotype (Fig. 3C, last two rows).

In ER+ breast cancer cells with amplification of WT HER2, there is clear evidence of crosstalk between the HER2 and ER signaling pathways (8,25). Thus, we next examined if non-amplified mutant HER2 was stimulating estradiol-independent ER transcriptional activity. Using an ERE (Estrogen Responsive Elements) luciferase reporter, baseline and estradiol-stimulated ER transcriptional reporter activity was overall no different in HER2 mutant vs. WT cells. Moreover, treatment with fulvestrant but not with neratinib abrogated basal and/or estradiol-induced transcriptional activity in all HER2 mutant cells (Figure 3D), further suggesting no interdependence of mutant HER2 and ER signaling in $MCF7^{L755S}$ and $MCF7^{V777L}$ cells. We next examined a real time (RT) Profiler array of 84 ER-regulated genes in $MCF7^{L755S}$ and $MCF7^{V777L}$ cells under estrogen deprived conditions. When compared to $MCF7^{WT}$ cells, cells harboring the *ERBB2* KD mutations showed modest changes in expression (≥2-fold) in only a small number of ER regulated genes. $MCF7^{V777L}$ exhibited modest upregulation in L1CAM, JUNB, and BCAR1, and downregulation in PGR1 (Figure 3E), while $MCF7^{L755S}$ exhibited upregulation in WISP2 and modest downregulation in FOXA1, CTSD1, and GPER1 (Supp. Figure S4). The absence of common genes between the two KD mutants suggests ER transcriptional activity does not play a role in the estrogen independent growth observed in both.

### *ERBB2* mutations hyperactivate and rely on PI3K/AKT/mTOR signaling.

HER2-dependent transformation and metastatic progression of breast cancer cells with WT HER2 gene amplification are mainly attributed to hyperactivation of the PI3K/AKT/mTOR survival pathway, with HER2/HER3 heterodimers being the most transforming of this receptor network (26,27). HER3, which lacks intrinsic kinase activity, is able to potently activate PI3K via its six docking sites for the p85 adaptor subunit of the PI3K dimer (28). Moreover, several approved HER2 antagonists exert their antitumor effect, at least in part, by inhibiting phosphorylation of HER3 and disabling PI3K/AKT/mTOR signaling (9,29). Further, phosphorylated HER3 was reported to be elevated in cells endogenously expressing the $ERBB2^{V777L}$ mutation compared to cells with WT HER2 (18). Thus, we next examined the role of HER3 in transformation induced by non-amplified mutant HER2. Immunoblot

analysis showed detectable Y1197 p-HER3 in MCF7$^{V777L}$ cells; treatment with fulvestrant resulted in a clear increase in p-HER3 in MCF7$^{L755S}$ and MCF7$^{V777L}$ cells (Figure 4A). This increase was abrogated by neratinib, suggesting it is due to HER2-mediated trans-activation of HER3. To determine whether HER3 function is causally associated with endocrine therapy resistance, we knocked down HER3 with two independent siRNAs. siRNA-mediated knockdown of HER3 was confirmed by immunoblot analysis of lysates from transfected MCF7$^{V777L}$ cells (Figure 4B). Monolayer growth analysis showed that transfection of HER3 siRNA resensitized MCF7$^{V777L}$ cells to fulvestrant (Figure 4C). HER3 activation requires heterodimerization with other ERBB family receptors. Immunoprecipitation of HER3 followed by HER2 immunoblot of HER3 antibody pulldowns revealed that both HER2 KD mutants exhibit higher levels of HER3:HER2 complexes (Figure 4D, E), further implying that ER+/HER2 mutant cells gain ER independent growth through enhanced activation of HER3.

Structural analysis of the HER2$^{V777L}$ by Bose *et al.* previously determined that the V777L mutation mirrored alterations observed in the EGFR regulatory DFG motif with altered kinase activity. These authors also proposed that HER2$^{L755S}$ adopts a confirmation that may sterically inhibit small molecule binding and in return could produce resistance to lapatinib (14). Thus, we next inquired a structural explanation for the apparent enhanced association of HER2$^{L755S}$ with HER3 using known HER2 and EGFR structures. While numerous crystal structures are available for EGFR, both in active and inactive states as well as bound to HER3, relatively few are available for HER2. Given the homologies in amino acid sequence (Supp. Figure S5), the proposed mechanism of activation of the HER2 kinase domain_ (30), and previously described structural analysis methods by Bose *et al.* (14), we compared both EGFR and HER2 structures (Figure 4F). HER2 residue L755 resides at the C-terminus of the β-strand prior to the regulatory αC helix in the kinase N-lobe. L755 is adjacent to the characteristic ion pair (K753/E770) whose formation of a salt bridge marks the active kinase conformation (31). HER3 binds the active EGFR kinase, forming an asymmetric heterodimer similar to activating homodimers of either EGFR or HER2 (30,32). Superposition of inactive EGFR and HER2 kinase structures with active EGFR structures alone or bound to HER3 highlighted the relative positions of the ion pair, αC helix and L755. Notably, L755 forms a stable hydrophobic core in the inactive conformations (Figure 4F, orange sidechains), while it appears more flexible in the active conformations (Figure 4F, magenta sidechains). This flexibility extends to the following loop, which helps form the HER3 binding site in the activating heterodimer. To examine if this observed flexibility is a general feature of active EGFR conformations, we compared the B-factors of sidechains corresponding to L755 in 122 available EGFR-like kinase structures (including mainly EGFR, two HER2, and four HER4) in either active or inactive conformations (Figure 4G). Indeed, the distribution of normalized B-factors for L755 shifted from average flexibility in inactive conformations to increased flexibility in active conformations, suggesting the HER2$^{L755S}$ conformation promotes increased binding with HER3.

### Inhibition of TORC1 *in vivo* restores sensitivity of MCF7$^{V777L}$ tumors to fulvestrant.

To identify differential intracellular signaling between cells with mutant vs. wild type HER2, we used an array of 43 phosphorylated human kinases phosphorylated intracellular proteins

in estrogen-deprived MCF7 cells. The main difference between both cell types was persistent phosphorylation of p70S6K (S6K) in $MCF7^{L755S}$ and $MCF7^{V777L}$ cells vs. $MCF7^{G309A}$ and $MCF7^{WT}$ cells (Figure 5A). Immunoblot analysis of S6, the downstream target of S6K, was also clearly higher in cells with *ERBB2* KD mutations in the presence or absence of estrogen (Figure 5B). Further interrogation of signal transducing molecules by immunoblot analysis revealed elevated levels of T308 p-AKT, S473 p-AKT and p-S6 in cells with *ERBB2* mutations, particularly in cells with cells with *ERBB2* KD mutations (Figure 5C). In $MCF7^{G309A}$ and $MCF7^{WT}$ cells but not in $MCF7^{L755S}$ and $MCF7^{V777L}$ cells, treatment with fulvestrant completely inhibited p-S6 levels. In $MCF7^{V777L}$ cells, treatment with neratinib did not affect p-S6 levels except in combination with fulvestrant (Figure 5C).

We next examined whether inhibition of signaling molecules altered in cells harboring *ERBB2* KD mutations would restore sensitivity to fulvestrant. For this purpose we used the PI3Kα inhibitor alpelisib, the TORC1 inhibitor everolimus and the MEK1/2 inhibitor selumetinib. Clonogenic growth assays showed treatment with alpelisib and everolimus, but not with selumetinib, restored the growth inhibitory action of fulvestrant (Figures 5D, Supp. Figure S6). Quantification revealed there was no statistically significant difference between alpelisib, everolimus, or neratinib when combined with fulvestrant (Supp. Figure S7). Further, immunoblot analysis of cell lysates showed that alpelisib and everolimus but not selumetinib, each in combination with fulvestrant completely abrogated p-S6 levels (Supp. Figure S8), supporting a role for PI3K/AKT/mTOR but not RAS/RAF/MEK/ERK signaling on mutant *ERBB2*-induced endocrine resistance. In each of these studies, we used doses of small molecules that effectively inhibited their molecular target, S473 p-AKT for alpelisib, p-S6 for everolimus, and p-ERK for selumetinib (Supp Fig S9–S11).

Finally, we extended these findings to studies in mice bearing HER2 mutant xenografts. Athymic ovariectomized mice with established $MCF7^{V777L}$ tumors were first treated with fulvestrant, which arrested tumor growth but did not induce tumor regressions (Figure 6A). In a second study, neratinib and fulvestrant, each alone, prevented tumor growth but only the combination induced regression of both $MCF7^{V777L}$ and $MCF7^{L755S}$ xenografts (Figure 6B, Supp. Figure S12). In a third experiment, mice with established $MCF7^{V777L}$ tumors were treated with fulvestrant alone or in combination with neratinib, alpelisib or everolimus. As observed in the *in vitro* growth experiments, there was no significant difference in tumor growth among any of the combinations with fulvestrant (Figure 6C). Finally, established $MCF7^{V777L}$ tumors were treated with everolimus, neratinib/everolimus, fulvestrant/everolimus or the triple combination of neratinib/fulvestrant/everolimus to determine the role of p-S6 in tumor progression. Similar to neratinib and fulvestrant, everolimus was modestly effective as a single agent. The combinations of neratinib/everolimus and neratinib/fulvestrant equally suppressed tumor progression and to a higher degree than single agent everolimus. Interestingly, treatment with the triple combination of neratinib, fulvestrant and everolimus induced close to complete tumor regression (Figure 6D). We speculate the incomplete inhibition of p-S6 by everolimus may be due to mTOR independent activation of S6K through mutant HER2-induced activation of RSK (33,34). IHC analysis of tumor sections revealed that treatment with the triple combination induced a significant decrease in p-S6 levels when compared to single-agent or any double combination, thus correlating with the near complete tumor responses observed (Supplemental Fig S13).

## Discussion

Although some mechanisms of endocrine therapy resistance in ER+ breast cancer have been well studied, several of these remain to be discovered and characterized. Here we report that *ERBB2* mutations are predominantly acquired in late stage ER+ breast cancer and may play an important role in the progression of estrogen independent ER+ tumors. It is generally accepted that in ER+ breast cancers with overexpression of WT HER2, there is molecular crosstalk between HER2 and ER signaling pathways, resulting in endocrine therapy resistance (35–38). Whether similar transactivation between these two pathways is operative in ER+/HER2 non-amplified mutant breast cancer cells is unclear. Our data suggested that *ERBB2* mutations are acquired in metastatic ER+ disease after exposure to endocrine therapy (Fig. 1). Hence, we examined herein the role of *ERBB2* mutations in endocrine resistance. Analysis of the cBioPortal and Genie databases revealed the *ERBB2* mutations have nearly complete mutual exclusivity from activating *ESR1* mutations (Supp. Figure S1) (5,6), suggesting that HER2 variants use may use an ERα-independent mechanism to mediate escape from estrogen suppression. Our studies with MCF7 cells with isogenically incorporated *ERBB2* mutations revealed that variants L755S and V777L in the kinase domain, but not G309A in the extracellular domain, generate estrogen independent growth and resistance to fulvestrant (Fig. 2). Combined with the clinical data, this result strongly supports *ERBB2* activating KD mutations are an acquired mechanism of endocrine therapy resistance.

Previous studies have demonstrated that patients with HER2-nonamplified breast cancer do not benefit from HER2-directed therapies (39). However, the identification of *ERBB2* mutations in breast cancers without HER2 gene amplification has led to clinical trials showing activity of HER2-directed therapies against these ‘low HER2’ tumors (40,41). The ongoing SUMMIT *ERBB2* Mutation Trial (ClinicalTrial identifier NCT01953926) identified neratinib as an effective drug against HER2 mutant breast and is currently assessing the efficacy of neratinib in combination with fulvestrant and trastuzumab (40,42). In this study, using in MCF7 cells harboring activating *ERBB2* KD mutations, we determined dual blockade of ER and HER2 signaling was required to achieve complete growth arrest and cell death (Fig. 3A, 5D). Very low levels of estrogen are observed in post-menopausal women. In order to recapitulate these conditions, we used picomolar levels of estradiol. These low levels of estradiol rescued cells with *ERBB2* KD mutations from neratinib action (Fig. 3C), further suggesting the need of simultaneously disabling ER and mutant HER2 function to achieve an optimal antitumor effect. Crosstalk between ER and HER2 signaling as well as the ability of HER2 to downregulate ER have been well characterized in ER+/HER2 amplified cells and tumors (43). The heterozygous, low copy incorporation of *ERBB2* mutations into the MCF7 genome used herein is biologically relevant to HER2 mutant tumors, as the overwhelming majority of these variants are not amplified in primary human tumors. In our studies, we found no evidence to suggest HER2 mutant signaling activates ER function and/or limits the effect of fulvestrant or estrogen deprivation on ER transcriptional activity (Figs. 2E, 2F, 3C, 3D, Supp. Fig. S4). This suggests, that unlike endocrine resistance drive by HER2 amplification (44), HER2 mutant tumors develop anti-ER therapy resistance independently of ER activity.

Induction of HER3 was previously identified as a mechanism for promoting re-expression of genes mediating endocrine resistant breast cancer cell growth (45). In line with this report, we found constitutively activated HER3 levels in MCF7$^{L755S}$ and MCF7$^{V777L}$ cells, particularly upon treatment with fulvestrant (Fig. 4A). HER3 is catalytically inactive and requires hetero-dimerization with other ERBB (HER) receptors. Upon dimerization, ERBB co-receptors phosphorylate HER3 which, in turn, can couple to signal transducers mainly the PI3K/AKT/mTOR pathway (44). Structural analysis of L755S HER2 suggested an increase in flexibility in the active state, thus allowing for an increased propensity for heterodimerization and activation of HER3. Mutation of L755 to serine replaces a hydrophobic sidechain that helps stabilize the N-lobe core in inactive EGFR-like kinases with a smaller hydrophilic side chain (Fig. 4F). The serine mutation increases solvent exposure of the sidechain in both EGFR and HER2 structures according to Site Directed Mutator (24) and allows the surrounding residues to become more solvent exposed, thus increasing flexibility (46). We propose this increased flexibility mimics that observed in activated states of EGFR-like kinase structures, thus shifting HER2 towards the activated state and enhancing its binding to HER3 (Fig. 4G). This would be consistent with the observed hyperactivity of the HER3/PI3K/AKT/mTOR axis in in MCF7$^{L755S}$ and MCF7$^{V777L}$ cells and its potential central role on the transformed phenotype induced by *ERBB2* activating mutations.

Inhibition of HER2 (with neratinib), TORC1 (with everolimus) or PI3Kα (with alpelisib) in combination with fulvestrant were equipotent *in vitro* (Fig. 5D) and *in vivo* (Fig. 6C); however, complete tumor regressions *in vivo* were only achieved with the triple combination of fulvestrant/neratinib/everolimus (Fig. 6D). IHC analysis revealed that inhibition of both TORC1 and mutant HER2 were required in order to achieve an optimal reduction in p-S6 levels (Supp. Fig. S13). Previous studies have shown that MCF7$^{V777L}$ cells exhibit increased PI3K signaling and cell migration (18). Further, online databases (cBioPortal, Genie) revealed that *ERBB2* mutations have a tendency to co-occur (Log Odds Ratio .323) with *PIK3CA* mutations (Supp. Fig. S1), suggesting a natural selection geared towards amplification of PI3K signaling. Combined with our data, these data also suggest that combinations of endocrine therapy with PI3K pathway inhibitors would be a rational strategy worthy of clinical investigation in cancers with activating *ERBB2* mutations.

In conclusion, we report herein that *ERBB2* activating mutations predominate in late stages of ER+ breast cancer after long-term ER suppression. These mutations led to estrogen independent growth and fulvestrant resistance with no significant changes in ER transcriptional activity. Dual blockade of HER2 and the ER pathways was necessary to effectively inhibit growth of ER+/HER2 mutant tumors. In addition, HER2 mutant signaling hyperactivated HER3/PI3K/AKT/mTOR, thus suggesting a causal association of aberrant activity of this pathway to endocrine resistance in patients with ER+/HER2 mutant breast cancer. Taken together, these studies suggest that patients with ER+/HER2 nonamplified breast cancerharboring *ERBB2* mutations would benefit from HER2 targeted therapies in combination with hormonal therapy.

## Supplementary Material

Refer to Web version on PubMed Central for supplementary material.

## Acknowledgements

We thank Teresa Dugger for general administration and technical assistance and Ariella Hanker for helpful discussions.

**Financial Support:** This study was funded by NIH Breast SPORE grant P50 CA098131, Vanderbilt-Ingram Cancer Center Support grant P30 CA68485, UT Southwestern Simmons Cancer Center Support Grant P30 CA142543, Susan G. Komen for the Cure Foundation grant SAC100013 (CLA), grants from the Breast Cancer Research Foundation (CLA), National Institutes of Health (GM094575 and GM127390 to NVG) and the Welch Foundation (I-1505 to NVG).

## References

1. Chia S, Gradishar W, Mauriac L, Bines J, Amant F, Federico M, et al. Double-blind, randomized placebo controlled trial of fulvestrant compared with exemestane after prior nonsteroidal aromatase inhibitor therapy in postmenopausal women with hormone receptor-positive, advanced breast cancer: results from EFECT. J Clin Oncol 2008;26:1664–70 [PubMed: 18316794]
2. Mauri D, Pavlidis N, Polyzos NP, Ioannidis JP. Survival with aromatase inhibitors and inactivators versus standard hormonal therapy in advanced breast cancer: meta-analysis. J Natl Cancer Inst 2006;98:1285–91 [PubMed: 16985247]
3. Lipton A, Leitzel K, Ali SM, Demers L, Harvey HA, Chaudri-Ross HA, et al. Serum HER-2/neu conversion to positive at the time of disease progression in patients with breast carcinoma on hormone therapy. Cancer 2005;104:257–63 [PubMed: 15952182]
4. Meng S, Tripathy D, Shete S, Ashfaq R, Haley B, Perkins S, et al. HER-2 gene amplification can be acquired as breast cancer progresses. Proc Natl Acad Sci U S A 2004;101:9393–8 [PubMed: 15194824]
5. Toy W, Shen Y, Won H, Green B, Sakr RA, Will M, et al. ESR1 ligand-binding domain mutations in hormone-resistant breast cancer. Nat Genet 2013;45:1439–45 [PubMed: 24185512]
6. Jeselsohn R, Buchwalter G, De Angelis C, Brown M, Schiff R. ESR1 mutations-a mechanism for acquired endocrine resistance in breast cancer. Nat Rev Clin Oncol 2015;12:573–83 [PubMed: 26122181]
7. Miller TW, Balko JM, Fox EM, Ghazoui Z, Dunbier A, Anderson H, et al. ERalpha-dependent E2F transcription can mediate resistance to estrogen deprivation in human breast cancer. Cancer Discov 2011;1:338–51 [PubMed: 22049316]
8. Gutierrez MC, Detre S, Johnston S, Mohsin SK, Shou J, Allred DC, et al. Molecular changes in tamoxifen-resistant breast cancer: relationship between estrogen receptor, HER-2, and p38 mitogen-activated protein kinase. J Clin Oncol 2005;23:2469–76 [PubMed: 15753463]
9. Arteaga CL, Engelman JA. ERBB receptors: from oncogene discovery to basic science to mechanism-based cancer therapeutics. Cancer Cell 2014;25:282–303 [PubMed: 24651011]
10. Yarden Y, Sliwkowski MX. Untangling the ErbB signalling network. Nat Rev Mol Cell Biol 2001;2:127–37 [PubMed: 11252954]
11. Cho HS, Mason K, Ramyar KX, Stanley AM, Gabelli SB, Denney DW, Jr., et al. Structure of the extracellular region of HER2 alone and in complex with the Herceptin Fab. Nature 2003;421:756–60 [PubMed: 12610629]
12. Garrett TP, McKern NM, Lou M, Elleman TC, Adams TE, Lovrecz GO, et al. The crystal structure of a truncated ErbB2 ectodomain reveals an active conformation, poised to interact with other ErbB receptors. Mol Cell 2003;11:495–505 [PubMed: 12620236]
13. Yarden Y, Pines G. The ERBB network: at last, cancer therapy meets systems biology. Nat Rev Cancer 2012;12:553–63 [PubMed: 22785351]

14. Bose R, Kavuri SM, Searleman AC, Shen W, Shen D, Koboldt DC, et al. Activating HER2 mutations in HER2 gene amplification negative breast cancer. Cancer Discov 2013;3:224–37 [PubMed: 23220880]
15. Lee JW, Soung YH, Seo SH, Kim SY, Park CH, Wang YP, et al. Somatic mutations of ERBB2 kinase domain in gastric, colorectal, and breast carcinomas. Clin Cancer Res 2006;12:57–61 [PubMed: 16397024]
16. Greulich H, Kaplan B, Mertins P, Chen TH, Tanaka KE, Yun CH, et al. Functional analysis of receptor tyrosine kinase mutations in lung cancer identifies oncogenic extracellular domain mutations of ERBB2. Proc Natl Acad Sci U S A 2012;109:14476–81 [PubMed: 22908275]
17. Hanker AB, Brewer MR, Sheehan JH, Koch JP, Sliwoski GR, Nagy R, et al. An Acquired HER2T798I Gatekeeper Mutation Induces Resistance to Neratinib in a Patient with HER2 Mutant-Driven Breast Cancer. Cancer Discov 2017;7:575–85 [PubMed: 28274957]
18. Zabransky DJ, Yankaskas CL, Cochran RL, Wong HY, Croessmann S, Chu D, et al. HER2 missense mutations have distinct effects on oncogenic signaling and migration. Proc Natl Acad Sci U S A 2015;112:E6205–14 [PubMed: 26508629]
19. Hanker AB, Estrada MV, Bianchini G, Moore PD, Zhao J, Cheng F, et al. Extracellular matrix/integrin signaling promotes resistance to combined inhibition of HER2 and PI3K in HER2+ breast cancer. Cancer Res 2017
20. Formisano L, Stauffer KM, Young CD, Bhola NE, Guerrero-Zotano AL, Jansen VM, et al. Association of FGFR1 with ERalpha Maintains Ligand-Independent ER Transcription and Mediates Resistance to Estrogen Deprivation in ER(+) Breast Cancer. Clin Cancer Res 2017;23:6138–50 [PubMed: 28751448]
21. Altschul SF, Madden TL, Schaffer AA, Zhang J, Zhang Z, Miller W, et al. Gapped BLAST and PSI-BLAST: a new generation of protein database search programs. Nucleic Acids Res 1997;25:3389–402 [PubMed: 9254694]
22. Cheng H, Schaeffer RD, Liao Y, Kinch LN, Pei J, Shi S, et al. ECOD: an evolutionary classification of protein domains. PLoS Comput Biol 2014;10:e1003926 [PubMed: 25474468]
23. Gerstein M A Resolution-Sensitive Procedure for Comparing Protein Surfaces and its Application to the Comparison of Antigen-Combining Sites. Acta Crystal 1992:271–6
24. Worth CL, Preissner R, Blundell TL. SDM--a server for predicting effects of mutations on protein stability and malfunction. Nucleic Acids Res 2011;39:W215–22 [PubMed: 21593128]
25. Arpino G, Wiechmann L, Osborne CK, Schiff R. Crosstalk between the estrogen receptor and the HER tyrosine kinase receptor family: molecular mechanism and clinical implications for endocrine therapy resistance. Endocr Rev 2008;29:217–33 [PubMed: 18216219]
26. Holbro T, Beerli RR, Maurer F, Koziczak M, Barbas CF, 3rd, Hynes NE. The ErbB2/ErbB3 heterodimer functions as an oncogenic unit: ErbB2 requires ErbB3 to drive breast tumor cell proliferation. Proc Natl Acad Sci U S A 2003;100:8933–8 [PubMed: 12853564]
27. Lee-Hoeflich ST, Crocker L, Yao E, Pham T, Munroe X, Hoeflich KP, et al. A central role for HER3 in HER2-amplified breast cancer: implications for targeted therapy. Cancer Res 2008;68:5878–87 [PubMed: 18632642]
28. Hellyer NJ, Kim MS, Koland JG. Heregulin-dependent activation of phosphoinositide 3-kinase and Akt via the ErbB2/ErbB3 co-receptor. J Biol Chem 2001;276:42153–61 [PubMed: 11546794]
29. Junttila TT, Akita RW, Parsons K, Fields C, Lewis Phillips GD, Friedman LS, et al. Ligand-independent HER2/HER3/PI3K complex is disrupted by trastuzumab and is effectively inhibited by the PI3K inhibitor GDC-0941. Cancer Cell 2009;15:429–40 [PubMed: 19411071]
30. Aertgeerts K, Skene R, Yano J, Sang BC, Zou H, Snell G, et al. Structural analysis of the mechanism of inhibition and allosteric activation of the kinase domain of HER2 protein. J Biol Chem 2011;286:18756–65 [PubMed: 21454582]
31. Stamos J, Sliwkowski MX, Eigenbrot C. Structure of the epidermal growth factor receptor kinase domain alone and in complex with a 4-anilinoquinazoline inhibitor. J Biol Chem 2002;277:46265–72 [PubMed: 12196540]
32. Littlefield P, Liu L, Mysore V, Shan Y, Shaw DE, Jura N. Structural analysis of the EGFR/HER3 heterodimer reveals the molecular basis for activating HER3 mutations. Sci Signal 2014;7:ra114 [PubMed: 25468994]

33. Roux PP, Shahbazian D, Vu H, Holz MK, Cohen MS, Taunton J, et al. RAS/ERK signaling promotes site-specific ribosomal protein S6 phosphorylation via RSK and stimulates cap-dependent translation. J Biol Chem 2007;282:14056–64 [PubMed: 17360704]
34. Garrett JT, Olivares MG, Rinehart C, Granja-Ingram ND, Sanchez V, Chakrabarty A, et al. Transcriptional and posttranslational up-regulation of HER3 (ErbB3) compensates for inhibition of the HER2 tyrosine kinase. Proc Natl Acad Sci U S A 2011;108:5021–6 [PubMed: 21385943]
35. Benz CC, Scott GK, Sarup JC, Johnson RM, Tripathy D, Coronado E, et al. Estrogen-dependent, tamoxifen-resistant tumorigenic growth of MCF-7 cells transfected with HER2/neu. Breast Cancer Res Treat 1992;24:85–95 [PubMed: 8095168]
36. Knowlden JM, Hutcheson IR, Jones HE, Madden T, Gee JM, Harper ME, et al. Elevated levels of epidermal growth factor receptor/c-erbB2 heterodimers mediate an autocrine growth regulatory pathway in tamoxifen-resistant MCF-7 cells. Endocrinology 2003;144:1032–44 [PubMed: 12586780]
37. Shou J, Massarweh S, Osborne CK, Wakeling AE, Ali S, Weiss H, et al. Mechanisms of tamoxifen resistance: increased estrogen receptor-HER2/neu cross-talk in ER/HER2-positive breast cancer. J Natl Cancer Inst 2004;96:926–35 [PubMed: 15199112]
38. Chung YL, Sheu ML, Yang SC, Lin CH, Yen SH. Resistance to tamoxifen-induced apoptosis is associated with direct interaction between Her2/neu and cell membrane estrogen receptor in breast cancer. Int J Cancer 2002;97:306–12 [PubMed: 11774281]
39. Vogel CL, Cobleigh MA, Tripathy D, Gutheil JC, Harris LN, Fehrenbacher L, et al. Efficacy and safety of trastuzumab as a single agent in first-line treatment of HER2-overexpressing metastatic breast cancer. J Clin Oncol 2002;20:719–26 [PubMed: 11821453]
40. Hyman DM, Piha-Paul SA, Won H, Rodon J, Saura C, Shapiro GI, et al. HER kinase inhibition in patients with HER2- and HER3-mutant cancers. Nature 2018;554:189–94 [PubMed: 29420467]
41. Ma CX, Bose R, Gao F, Freedman RA, Telli ML, Kimmick G, et al. Neratinib Efficacy and Circulating Tumor DNA Detection of HER2 Mutations in HER2 Nonamplified Metastatic Breast Cancer. Clin Cancer Res 2017;23:5687–95 [PubMed: 28679771]
42. Gandhi L, Bahleda R, Tolaney SM, Kwak EL, Cleary JM, Pandya SS, et al. Phase I study of neratinib in combination with temsirolimus in patients with human epidermal growth factor receptor 2-dependent and other solid tumors. J Clin Oncol 2014;32:68–75 [PubMed: 24323026]
43. Nahta R, O'Regan RM. Therapeutic implications of estrogen receptor signaling in HER2-positive breast cancers. Breast Cancer Res Treat 2012;135:39–48 [PubMed: 22527112]
44. Osborne CK, Schiff R. Mechanisms of endocrine resistance in breast cancer. Annu Rev Med 2011;62:233–47 [PubMed: 20887199]
45. Hutcheson IR, Goddard L, Barrow D, McClelland RA, Francies HE, Knowlden JM, et al. Fulvestrant-induced expression of ErbB3 and ErbB4 receptors sensitizes oestrogen receptor-positive breast cancer cells to heregulin beta1. Breast Cancer Res 2011;13:R29 [PubMed: 21396094]
46. Zhang H, Zhang T, Chen K, Shen S, Ruan J, Kurgan L. On the relation between residue flexibility and local solvent accessibility in proteins. Proteins 2009;76:617–36 [PubMed: 19274736]

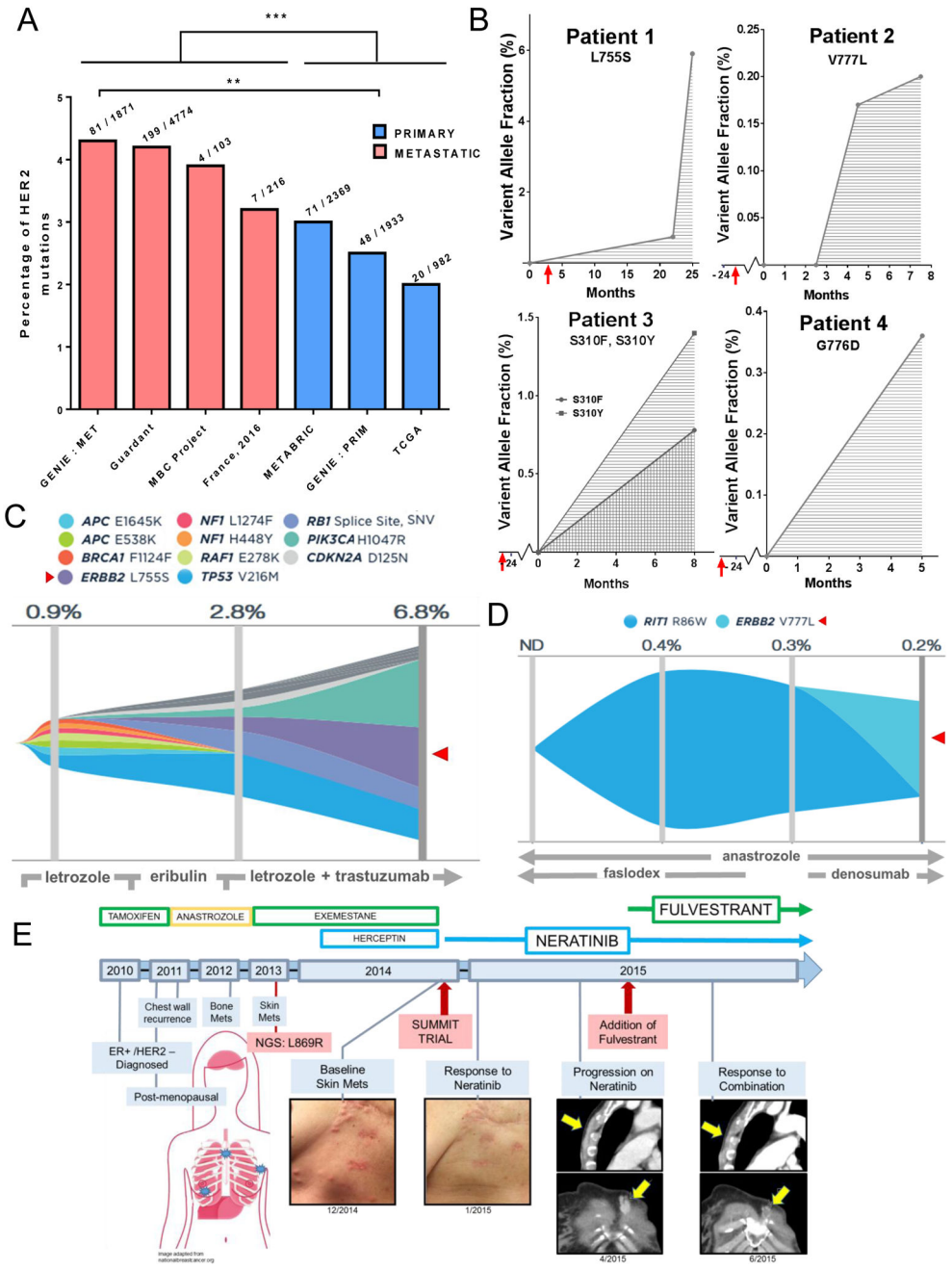


**Fig. 1. *ERBB2* mutations predominantly occur in ER+ breast cancer after progression on endocrine therapy.**

(A) Percent of *ERBB2* mutations stratified by tumor type (primary vs metastatic) using online databases in cBioPortal (GENIE, TCGA, METABRIC, MBC Project, and France 2016) and the Guardant Health database. Statistical analysis was carried out comparing the frequency of *ERBB2* mutations in primary vs metastatic tumors (in the case of Guardant Health in plasma from patients with or without metastatic disease) of all pooled databases (***p<0.001, chi-square test with Yates' correction), and among the GENIE database, separately (**p<0.01, chi-square test with Yate's correction). Numbers above each bar graph

indicate *ERBB2* mutations over sample size in the denominator. B) Plasma tumor ctDNA in the Guardant Health database from patients with ER+/HER2-negative (HER2 non-amplified) breast cancer that developed *ERBB2* mutations after extended periods of endocrine therapy. Red arrows indicate the start of endocrine therapy. Time point 0 represents the first analysis of plasma ctDNA. (C) Mutational landscape of Guardant patient 1 with cancer harboring $ERBB2^{L755S}$ (red arrow) with corresponding treatment course. Please note that this patient's tumor was not HER2 amplified but received trastuzumab after the emergence of the L755S mutation. (D) Mutational landscape of Guardant patient 2 with cancer harboring $ERBB2^{V777L}$ (red arrow) with corresponding treatment course. (E) Clinical course of patient with ER+ lobular breast cancer with $ERBB2^{L869R}$ after primary treatment with aromatase inhibitors. Following excellent response to neratinib, patient progressed with new bone and lymph node metastases. Upon addition of fulvestrant to neratinib, patient exhibited a prolonged response to the combination.

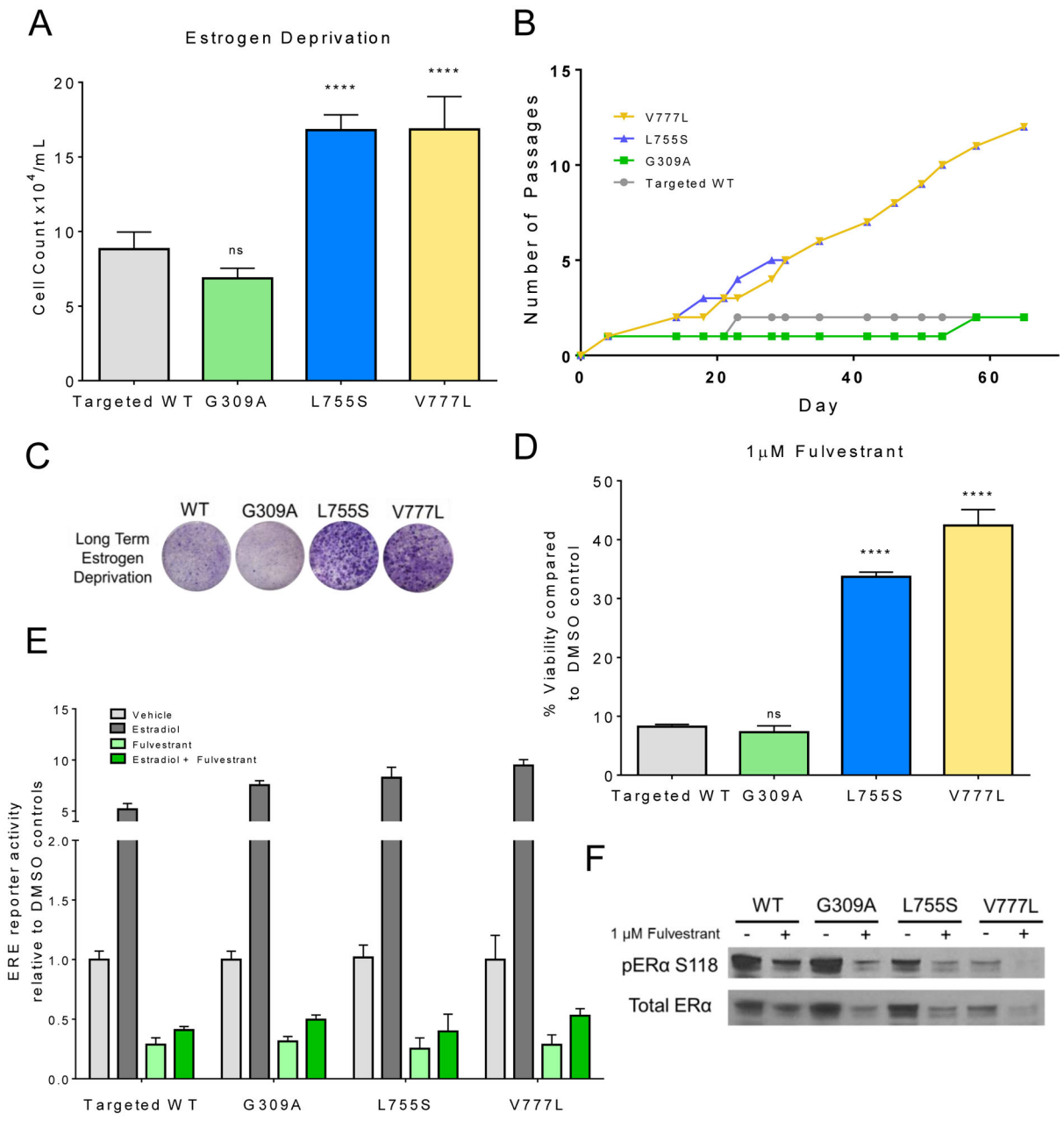


**Fig. 2. Activating *ERBB2* mutations generate resistance to anti-ER therapies.**

(A) Isogenically modified MCF7 cells with incorporated $HER2^{WT}$ (targeted WT), $ERBB2^{G309A}$, $ERBB2^{L755S}$ and $ERBB2^{V777L}$ into the host genome, were grown in estrogen deprived medium [5% charcoal-stripped serum (CSS), phenol-red free]. Cell counts were taken on day 8. Data represent the average ± SD of 3 replicate wells. Statistical comparisons were between HER2 mutant and HER WT cells (****$p<0.0001$, ANOVA). Experiment was repeated 3 times. (B) Growth in estrogen-deprived medium (60 days) was carried out in 100-mm dishes. Passage number was recorded for each cell line. (C) Representative crystal violet-stained monolayers of cells grown for 28 days in estrogen-deprived medium. (D) Cells were treated with 1 μM fulvestrant in medium containing 10% FBS. Cell counts were

taken on day 8 and are shown as % of vehicle-treated controls for each cell line. Data represent the average ± SD of 3 replicate wells. Statistical comparisons were between HER2 mutant and HER WT cells (****p<.0001, ANOVA). Experiment was repeated 3 times. (E) Cells were plated in estrogen deprived medium and transfected with pERE (Estrogen Responsive Elements)-luciferase and pCMV-Renilla plasmids; 24 h post transfection, cells were treated ± 1 nM estradiol ± 1 μM fulvestrant. Luciferase activity was measured 24 h later using the Dual Luciferase Kit (Promega) as described in Methods. Data represent the average ± SD of 4 replicate wells. The experiment was repeated three times. (F) Cells were grown in full medium ± 1 μM fulvestrant for 24 h. Cell lysates were prepared and subjected to immunoblot analyses with the indicated antibodies.

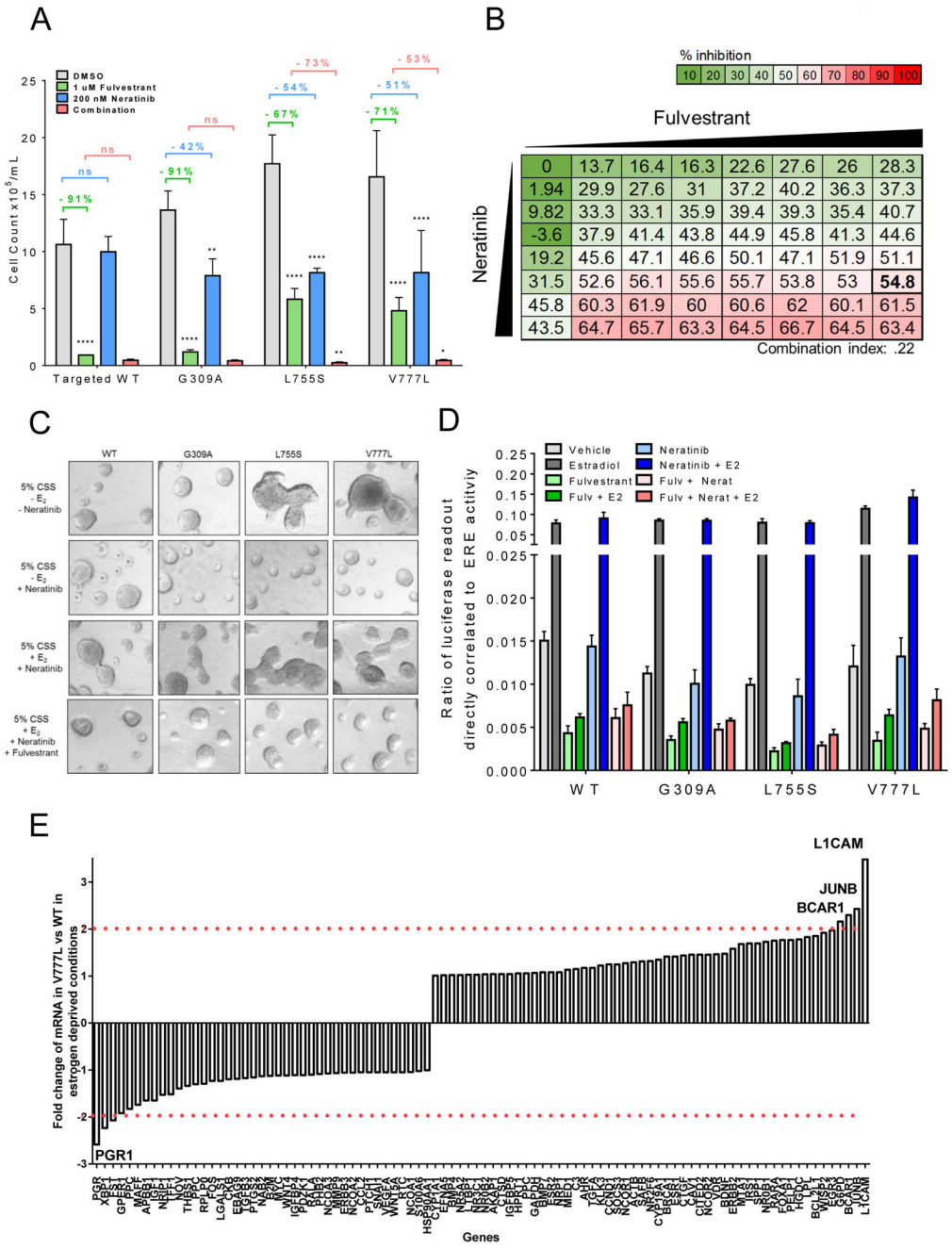


**Fig. 3. Dual blockade of ER and HER2 in ER+/HER2-mutant cells.**

(A) The indicated cells were grown in complete medium ± 1 μM fulvestrant ± 200 nM neratinib. Cell counts were taken on day 12. Data represent the average ± SD of 3 replicate wells. Statistical comparison between HER2 mutant cells treated with single drugs and DMSO-treated controls are shown as percent reduction (**p<0.01, ****p<0.0001, ANOVA with Tukey's multiple comparison). For the combination of neratinib/fulvestrant (red), statistical comparisons were to fulvestrant (green) (*p<0.05, **p<0.01, ANOVA with Tukey's multiple comparison). Experiment was repeated 3 times. (B) Synergistic growth assay. MCF7$^{V777L}$ were treated with a dose range (0, 31.25 nM, 62.5 nM, 125 nM, 250 nM,

500 nM, and 1000 nM) of fulvestrant and neratinib alone and in combination. Data represent the average of 3 replicate plates. The combination Index value 1 μM fulvestrant and 250 nM neratinib (indicated by the bold box) was .22 and considered to be synergistic. (C) The indicated cells were plated in 3D matrigel. Estrogen deprived media ± 1 nM estradiol ± 1 μM fulvestrant ± 200 nM neratinib, was used as indicated. Media and growth factors were changed every 3 days. Colonies (≥50 μM) were imaged on Day 12. Representative images shown. Assay was carried out in duplicate wells in 3 separate experiments. (D) Cells were plated in estrogen deprived medium and transfected with pERE (Estrogen Responsive Elements)-luciferase and pCMV-Renilla plasmids; 24 h post transfection, cells were treated ± 1 nM estradiol ± 1 μM fulvestrant ± 200 nM neratinib. Luciferase activity was measured 24 h later using the Dual Luciferase Kit (Promega) as described in Methods. Data represent the average ± SD of 4 replicate wells. The experiment was repeated three times. (E) Gene expression analysis using Reverse Transcription (RT) Profiler of genes regulated by ERα in $MCF^{WT}$ and $MCF7^{V777L}$ cells as described in Methods. Bar graphs are an average of 3 separate wells. Fold change in gene expression between $MCF7^{V777L}$ and $MCF^{WT}$ cells is plotted in the Y axis. Genes with a change in expression ≥2 are labeled.

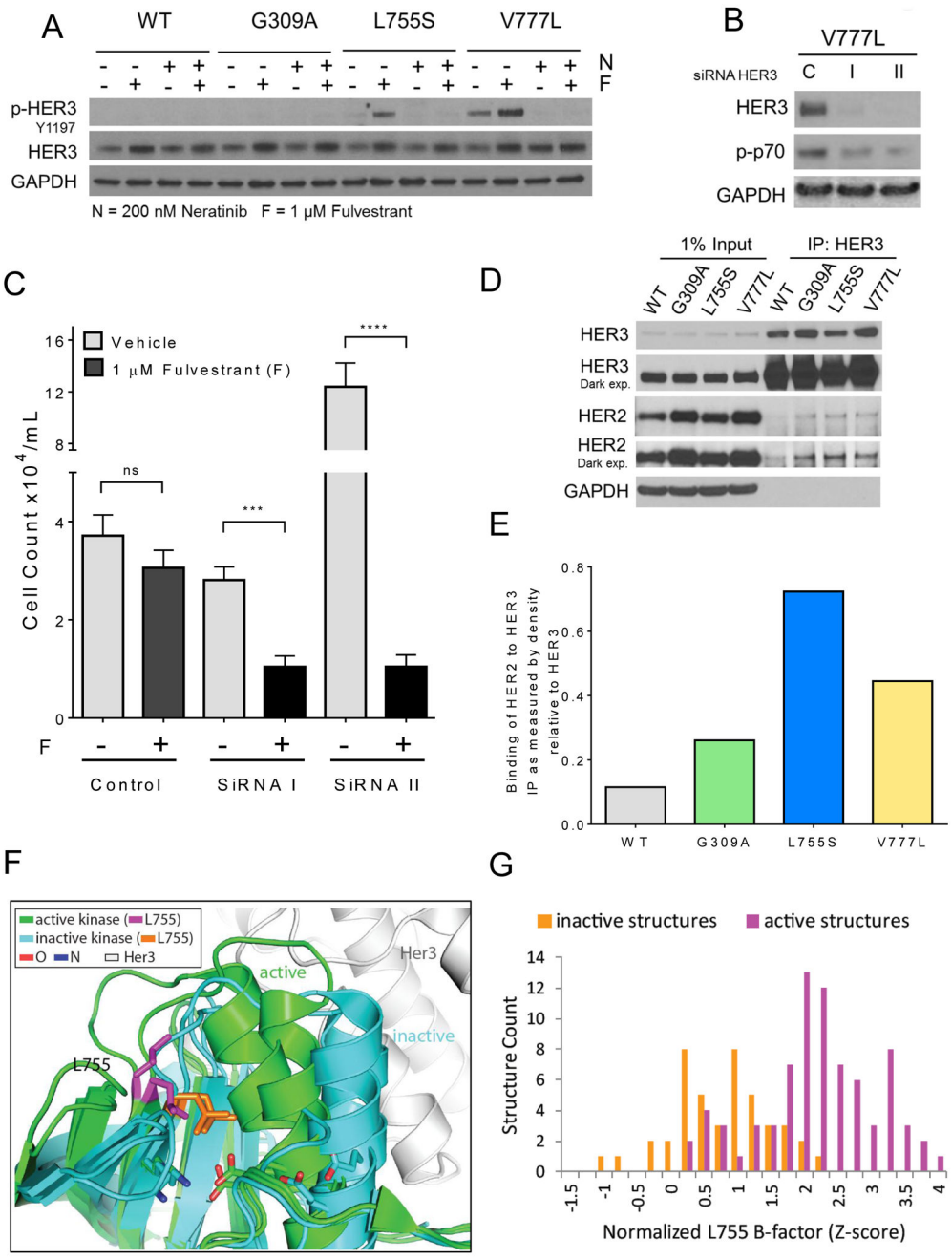


**Fig. 4. HER3 activation and endocrine resistance in HER2 mutant cells.**

(A) Cells were grown in full medium ± 1 μM fulvestrant (F) ± 200 nM neratinib (N) for 24 h. Cell lysates were prepared and subjected to immunoblot analyses with the indicated antibodies. (B) *ERBB2*$^{V777L}$ cells were plated in 100-mm dishes and transfected with 2 different HER3 (I, II) or control (c) siRNAs as described in Methods. Cell lysates were harvested 3 days post-transfection. Immunoblot analysis of HER3 confirmed knockdown in HER3. (C) Quantification of of MCF7$^{V777L}$ cells ± 1 μM fulvestrant (F) ± HER3 siRNAs. Six days after plating, monolayers were harvested and cell counts determined using a Coulter Counter. Each bar represents the mean cell number ± SD of triplicate wells

(***p<0.001, ****p<.0001, ANOVA). (D) HER3/HER2 co-immunoprecipitation in lysates from the indicated cells. Protein (1 mg) was isolated and immunoprecipitated (IP) with 1 μg of a C-terminal HER3 antibody. Antibody pulldowns were separated by SDS-PAGE, transferred to nitrocellulose, and subjected to immunoblot analysis (IB) with the indicated antibodies. (E) HER2:HER3 ratio of immunoreactive bands quantified using ImageJ (Y axis). (F) Superposition of HER1 in the active (green) and inactive (cyan) confirmations. L755 residue shown as the active (magenta) and inactive (orange) residues. Oxygen (O, red) and Nitrogen (N, blue) sites are indicated with respective colors. (G) Quantification of the flexibility (B-factor) of the L755S mutant in the active state (magenta) vs inactive state (orange). Flexibility is directly correlated to the ability to bind to HER3.

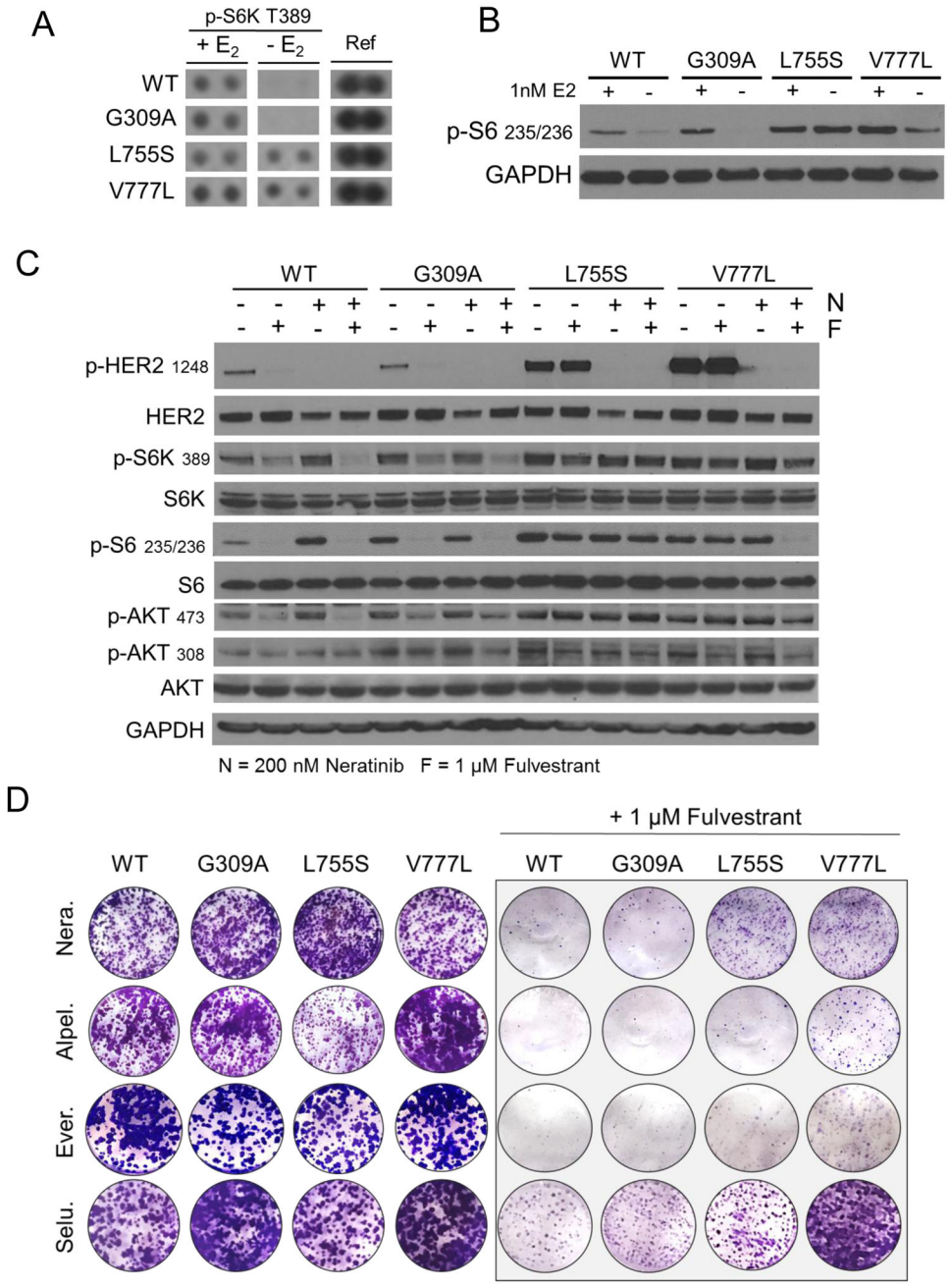


**Fig. 5. *ERBB2* kinase domain mutations hyperactivate the PI3K/AKT/m TOR pathway.**

(A) Phospho-kinase array of lysates from MCF7/HER2 mutant cells grown in IMEM phenol-red free medium, 5% CSS FBS ± 1 nM estradiol ($E_2$). Lysates and blots were processed following the manufacturer's instructions. S6K site T389 shown next to positive control reference (Ref) spots. (B) Immunoblot to confirm array results. The indicated cells were grown in IMEM phenol-red free medium ± 1 nM estradiol overnight. Cell lysates were prepared and subjected to immunoblot analyses with the indicated antibodies. (C) The indicated MCF7 cells were grown in full medium ± 1 μM fulvestrant (F) ± 200 nM neratinib (N). Cell lysates were subjected to immunoblot analyses with the indicated antibodies. (D)

Cells were seeded in full medium with 200 nM neratinib, 1 μM alpelisib, 25 nM everolimus, or 1 μM selumetinib, as indicated, ± 1 μM fulvestrant. Cells were seeded in triplicate in 12-well plates and stained on day 10 with crystal violet and imaging intensity of stained monolayers quantitated as described in Methods.

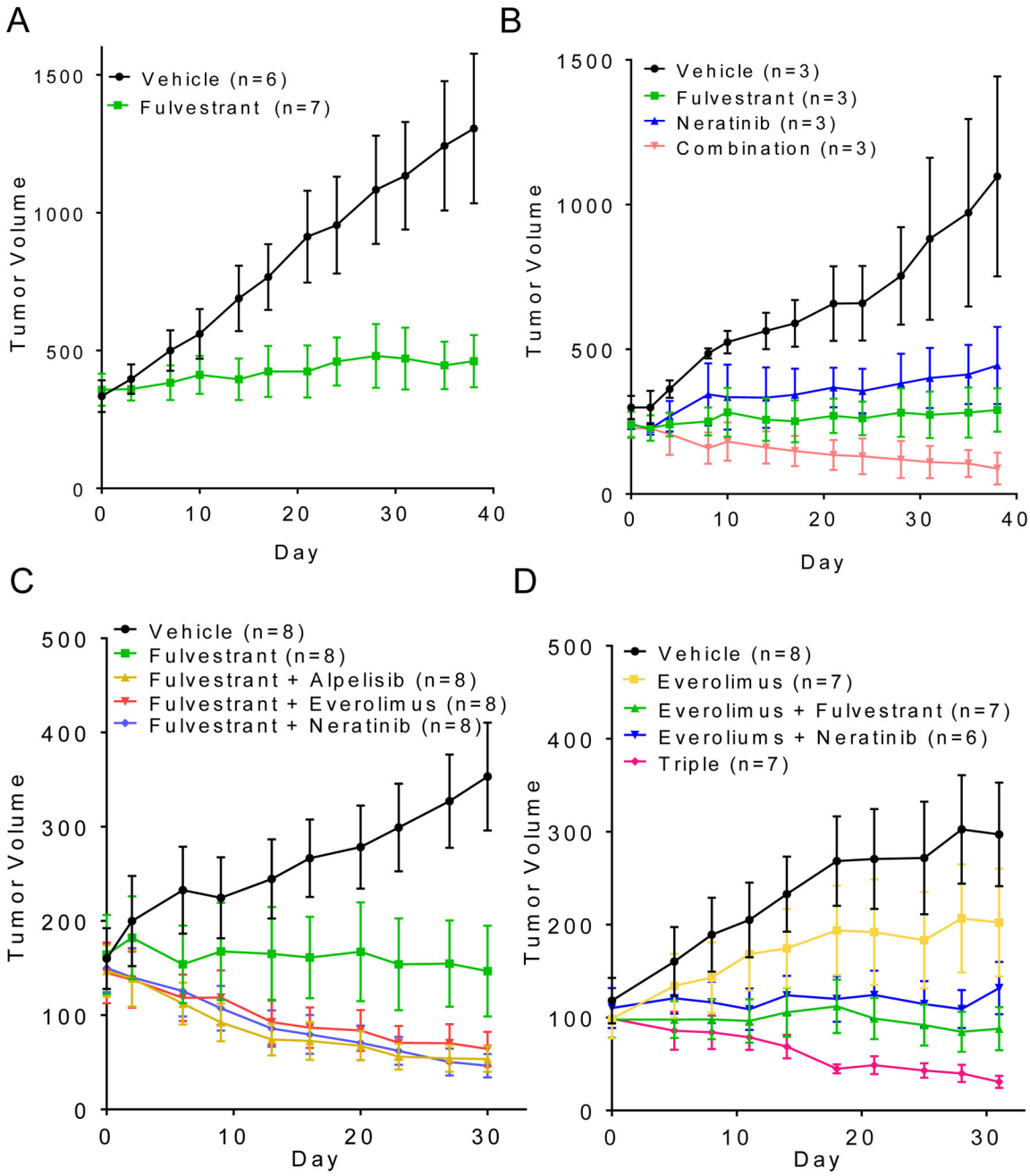


**Fig. 6. MCF7 xenografts harboring *ERBB2*$^{V777L}$ respond to dual blockade of HER2 and ER.**

(A) MCF7$^{V777L}$ xenografts were established s.c. in ovariectomized athymic mice supplemented with a 28-day release, 0.25-mg 17β-estradiol pellet. Once tumors reached approximately 200 mm$^3$, mice were randomized to treatment with vehicle or fulvestrant (5 mg/kg/week). Each data point represents the mean tumor volume in mm$^3$ ± SD. (B) MCF7$^{V777L}$ xenografts were established as in (A) following implantation of a s.c. 14-day release, 0.25-mg 17β-estradiol pellet. Once tumors reached approximately 200 mm$^3$, mice were randomized to treatment with vehicle, fulvestrant (5 mg/kg/week), neratinib (40 mg/kg/day), or both drugs for 5 weeks. Each data point represents the mean tumor volume in

$mm^3$ ± SD. (C) $MCF7^{V777L}$ xenografts were established in mice as in (B); once tumors reached ≥100 $mm^3$, mice were randomized to treatment with vehicle, fulvestrant (5 mg/kg/week), alpelisib (30 mg/kg/day) + fulvestrant, everolimus (5 mg/kg/day) + fulvestrant, or neratinib (40 mg/kg/day) + fulvestrant for 5 weeks. Each data point represents the mean tumor volume in $mm^3$ ± SD. (D) $MCF7^{V777L}$ xenografts were established in mice as in (B); once tumors reached ≥100 $mm^3$, mice were randomized to treatment with vehicle, everolimus (5 mg/kg/day), everolimus + fulvestrant (5 mg/kg/week), everolimus + neratinib (40 mg/kg/day), or all three drugs for 5 weeks. Each data point represents the mean tumor volume in $mm^3$ ± SD. Number in mice per treatment are shown in parentheses.